Available online at www.sciencedirect.com
SCIENCE DIRECT®
Icarus 175 (2005) 141–158
ICARUS
www.elsevier.com/locate/icarus

Near-IR spectral evidence for the presence of iron-poor orthopyroxenes on the surfaces of six M-type asteroids

Paul S. Hardersen [a,*,1], Michael J. Gaffey [b,1], Paul A. Abell [c,1,2]

[a] *Department of Space Studies, Room 526, Box 9008, University of North Dakota, Grand Forks, ND 58202, USA*
[b] *Department of Space Studies, Room 518, Box 9008, University of North Dakota, Grand Forks, ND 58202, USA*
[c] *NASA Johnson Space Center, Mail Code SR, Houston, TX 77058, USA*

Received 8 April 2004; revised 11 October 2004

Available online 22 January 2005

Abstract

The first verifiable near-infrared absorption features in the ∼ 0.9-μm spectral region are reported for Asteroids 16 Psyche, 69 Hesperia, 110 Lydia, 125 Liberatrix, 201 Penelope, and 216 Kleopatra. These weak features (∼ 1–3%) are attributed to orthopyroxenes present on the surfaces of these asteroids. 16 Psyche and 125 Liberatrix have full rotational coverage while 69 Hesperia, 110 Lydia, 201 Penelope, and 216 Kleopatra have ∼ 75% rotational coverage. Qualitative ∼ 2-μm absorption features are present, but are very weak (< 1%). Absorption band positions suggest relatively low abundances of calcium and iron in the pyroxenes. This indicates relatively reducing redox conditions for these asteroids, their parent bodies, and the nebular regions in which they formed. Four potential interpretations for these asteroids include: (1) they are exposed metallic cores or core fragments of differentiated parent bodies with residual orthopyroxene mantle material, (2) they are the result of a smelting-like reaction that converts olivine to pyroxene and metallic iron in the presence of carbon at high temperatures, (3) they are analogs to the primitive metal-rich Bencubbinite meteorites, or (4) they represent metallic surfaces which have accumulated silicate debris from external sources. Of the two original interpretations for the M-asteroids, the enstatite chondrite interpretation (Chapman and Salisbury, 1973, Icarus 19, 507–522; Gaffey and McCord, 1979, Mineralogical and petrological characterizations of asteroids. In: Gehrels T. (Ed.), Asteroids. Univ. of Arizona Press, Tucson, pp. 688–723) can be eliminated for these asteroids because the pyroxene in enstatite chondrites is iron-free and does not exhibit such absorption features. The iron meteorite interpretation remains valid, but with modification. For M-Asteroids 16 Psyche and 216 Kleopatra, these spectral results combined with previous determinations of high radar albedos indicate that these bodies are most probably exposed core fragments of differentiated bodies. M-Asteroids 69 Hesperia, 110 Lydia, 125 Liberatrix, and 201 Penelope exhibit similar spectral features consistent with exposed core fragments, but radar observations would be needed to confirm a high metal abundance. Observations of M-Asteroids 136 Austria and 325 Heidelberga suggest the absence of absorption features in the ∼ 0.4- to ∼ 2.5-μm region within the scatter of the data. Verification of the presence or absence of features across the surfaces of these two asteroids requires full rotational coverage. The interpretations for these "featureless" M-asteroids are not well-constrained, but remain consistent with the iron meteorite and enstatite chondrite interpretations.

Keywords: Asteroids, composition; Mineralogy; Spectroscopy; Infrared observations; Iron meteorites, parent bodies

1. Introduction

The M-type asteroids are one of 14 distinct taxonomic groupings that originate from the work of Tholen (1984, 1989) and represent a group of asteroids that has been historically difficult to interpret due to the apparent lack of diagnostic mineral absorption features in their visible- and near-infrared reflectance spectra. Derived from the larger group

* Corresponding author. Fax: +1-701-777-3711.
E-mail address: hardersen@volcano.space.edu (P.S. Hardersen).

[1] Visiting astronomer at the Infrared Telescope Facility, which is operated by the University of Hawaii under Cooperative Agreement No. NCC 5-538 with the National Aeronautics and Space Administration, Office of Space Science, Planetary Astronomy Program.

[2] National Research Council Associate.

0019-1035/$ – see front matter
doi:10.1016/j.icarus.2004.10.017

Table 1
Taxonomy comparisons of the M-asteroids

Asteroid		Asteroid	Tholen class	Barucci class	Tedesco class	Howell class	Bus class
16	Psyche	0.1203	M	M0	M	M	X
21	Lutetia	0.2212	M	M0	M	M	Xk
22	Kalliope	0.1419	M	M0	M	M	X
55	Pandora	0.3013	M	E0	E?	–	X
69	Hesperia	0.1402	M	M0	M	M	X
75	Eurydike	0.1486	M	M0	M	–	Xk
77	Frigga	0.1440	MU	D2	M?	–	Xe
97	Klotho	0.2285	MU	M0	M	–	–
110	Lydia	0.1808	M	M0	M	–	X
125	Liberatrix	0.2253	MU	M0	M	–	X
129	Antigone	N/A	M	–	–	–	X
132	Aethra	0.1718	M	M0	M?	–	Xe
135	Hertha	0.1436	M	M0	M	M,T	Xk
136	Austria	0.1459	M	–	–	–	Xe
161	Athor	0.1980	M	M0	M	–	Xc
201	Penelope	0.1604	M	M0	M	–	X
216	Kleopatra	0.1164	M	M0	M	–	Xe
224	Oceana	0.1694	M	–	–	–	–
250	Bettina	0.2581	M	M0	M	–	Xk
325	Heidelberga	0.1068	M	–	–	–	–
338	Budrosa	0.1766	M	M0	M	–	Xk
347	Pariana	0.1751	M	M0	M	–	–
369	Aeria	0.1919	M	M0	M	–	–
382	Dodona	0.1610	M	M0	M	–	–
413	Edburga	0.1466	M	–	–	–	X
418	Alemannia	0.1878	M	M0	–	–	–
441	Bathilde	0.1410	M	–	–	–	Xk
497	Iva	N/A	M	–	–	–	–
498	Tokio	0.0679	M	D3	T	–	–
516	Amherstia	0.1627	M	–	–	–	X
558	Carmen	0.1161	M	M0	M	–	–
572	Rebekka[a]	0.0847	XDC	–	–	–	C
755	Quintilla	0.1621	M	M0	–	–	–
766	Moguntia	0.1572	MU	–	–	–	–
785	Zwetana	0.1245	M	B2	M	–	Cb
796	Sarita[a]	0.1966	XD	–	–	–	X
798	Ruth	0.1583	M	–	–	–	–
849	Ara	0.2660	M	–	–	M	–
857	Glasenappia	0.2318	MU	–	–	–	–
860	Ursina	0.1618	M	M0	–	–	X
872	Holda	0.2127	M	–	–	–	X
931	Whittemora	0.1704	M	M0	–	–	–
1210	Morosovia	0.1695	MU:	–	–	–	–
1461	Jean-Jacques	0.1582	M	M0	–	–	–

Notes. Tholen class taken from Tholen (1984, 1989). Albedo information from PDS Small Bodies Node, data from IRAS. Bus class taken from Bus and Binzel (2002). Barucci class taken from Barucci et al. (1987). Howell class taken from Howell et al. (1994). Tedesco class taken from Tedesco et al. (1989).
[a] Reclassified as M-asteroid in Rivkin et al. (1995).

of X-class asteroids that represent spectrally featureless, moderately "reddish" objects in the 0.3- to 1.1-μm region (Tholen, 1984), the M-asteroids are distinguished by exhibiting moderate albedos (∼ 0.07 to 0.30). The other members of the X-group, the E- and P-type asteroids, exhibit higher and lower albedos, respectively (Tholen, 1984). Other taxonomic classification schemes (Barucci et al., 1987; Tedesco et al., 1989; Burbine, 1991; Howell et al., 1994) have generally produced results similar to those of Tholen (1984, 1989). However, since these asteroid classifications do not depend on compositionally-diagnostic parameters, different asteroid taxonomic systems differ depending on which observational parameters are used to define the taxonomy. A comparison of the classifications of M-asteroids across different taxonomic schemes is given in Table 1.

Several spectral surveys undertaken in the past 20 years have observed M-asteroids at both visible- and near-infrared wavelengths (Chapman and Gaffey, 1979; Zellner et al., 1985; Bell et al., 1988; Clark et al., 1995; Xu et al., 1995; Bus, 1999; Bus and Binzel, 2002; Rivkin et al., 1995, 2000). Prior to 2002, there have been no published reports of verified spectral absorption features in the visible and near-infrared (∼ 0.4 to 2.5 μm) spectra of any M-asteroids. However, spectra for M-asteroids from some of these sur-

veys show tantalizing hints that weak features may exist. For example, the 52-color survey (Bell et al., 1988) shows the possibility of weak ∼ 0.9-μm features for 16 Psyche, 22 Kalliope, 69 Hesperia, and 135 Hertha. Additionally, SMASS II data from Bus (1999) and Bus and Binzel (2002) suggest weak features for 69 Hesperia and 201 Penelope.

Based on the possibility that weak features exist in the spectra of some M-asteroids and following the commissioning of the SpeX near-infrared spectrograph at the NASA Infrared Telescope Facility (IRTF) in 2001, we undertook an observing program to study a subset of the M-asteroids to determine if their spectra exhibit any mineralogically diagnostic absorption features in the ∼ 0.8- to 2.5-μm spectral region. These near-infrared absorption features are caused by the presence of the Fe^{2+} cation within the crystal structure of cosmochemically important mafic minerals, such as olivine, pyroxene, spinel, and feldspar (Burns, 1993). The lack of iron-bearing minerals on an asteroid's surface will preclude the formation of these absorption features. Detection of these features is important because it allows the identification of mafic minerals and determination of their mineral chemistries and abundances on asteroid surfaces. This allows asteroid surface mineralogies to be more rigorously constrained and results in more robust inferences concerning the chemical, mineralogical, geological, and thermal histories of individual asteroid parent bodies.

The apparently featureless spectra of M-asteroids led workers to suggest that either enstatite chondrites or NiFe meteorites were the best analogs for the M-type asteroids (Chapman and Salisbury, 1973; Gaffey and McCord, 1979). These inferences are based on the general similarities between M-asteroid spectra and the spectra of these meteorite types, although specific diagnostic features were lacking (Chapman and Salisbury, 1973; Gaffey and McCord, 1979). More recent studies suggest that some M-asteroids have phyllosilicate-rich surfaces due to the presence of absorptions in the 3-μm region of the spectrum (Rivkin et al. 1995, 2000).

All three interpretations are viable since the available visible and near-infrared survey spectra of most M-asteroids do not exhibit diagnostic spectral features. However, detections of weak—but verifiable and repeatable—diagnostic absorption features associated with specific minerals would strongly constrain the surface mineralogies of these asteroids. This, in turn, will constrain the histories of the asteroids' parent bodies and the conditions in which they formed.

The previous interpretations, whether enstatite chondrites, NiFe metal, or phyllosilicate minerals, imply very different formation conditions for individual M-asteroids. While it is probable that all three interpretations are correct for subsets of the M-population (Gaffey et al., 1993), the actual composition for each M-asteroid must be determined to establish its affinities and history. Each interpretation suggests a unique thermal regime. Abundant phyllosilicate minerals suggest a relatively low-level of heating (∼ 0 to 300 °C, Keil, 2000); an enstatite-chondrite-like asteroid could have experienced thermal regimes ranging from no heating to strong thermal metamorphism (Keil, 1989); and the NiFe metal-rich assemblage suggests a high temperature environment associated with the core of a differentiated parent body. Significant advances in understanding the thermal history of the main asteroid belt will greatly benefit from better compositional constraints for all "featureless" asteroids, including the M-asteroids.

2. Observations and data reduction

2.1. Observations

Eight M-asteroids were investigated during two observing runs at the IRTF on Mauna Kea, Hawaii. The first observing run took place from April 29 through May 4, 2001; the second observing run occurred from March 22 through 25, 2002. Both runs utilized the SpeX near-infrared spectrograph to observe these asteroids in the low-resolution (asteroid mode, $R = 93.75$) from ∼ 0.8 to 2.5 μm (Rayner et al., 2003). Two half-nights of observing during the first run and two full nights during the second run were lost due to clouds and fog. All remaining nights were photometric and allowed acquisition of the data presented in this paper.

69 Hesperia, 110 Lydia, 201 Penelope, and 216 Kleopatra were observed on multiple nights during the 2001 observing run. Asteroid 325 Heidelberga was also observed on the first night of the same run. Table 2 lists the average observational parameters for each asteroid. For all asteroids except 325 Heidelberga, the observational goal involved obtaining rotationally-resolved spectra over at least one full rotation period. The purpose of the rotational coverage was to search for variations in any spectral absorption features that are present. Asteroids with relatively short rotation periods ($\lesssim$ 6 h) make this task much easier—and 69 Hesperia, 201 Penelope, and 216 Kleopatra all have periods less than six hours. The rotational data obtained from each of the four primary asteroids observed during this run covers ∼ 75% of their surfaces. 325 Heidelberga received limited attention on the first night of the run with the acquisition of four spectra.

16 Psyche, 125 Liberatrix, and 136 Austria were observed during the second observing run in March 2002. Both 16 Psyche and 125 Liberatrix were observed through about one full rotational period—16 Psyche on March 22 and 125 Liberatrix on March 23. 136 Austria received ∼ 36% rotational coverage from spectra obtained on March 22. Table 3 includes physical and dynamical information for all asteroids discussed in this paper.

For both runs, the observational strategy included the acquisition of spectra of the asteroids, local standard stars, and solar analog stars. The local standard stars can also be termed extinction stars because they are observed multiple times during an evening so that empirical, wavelength-

Table 2
Average observational parameters for M-asteroids in this paper

Asteroid		Right ascension	Declination	Apparent V mag	Solar distance (AU)	Phase angle (°)	Total spectra
16	Psyche	$10^h37^m4.12^s$	9°54′3.50″	10.74	3.232	7.12	120
69	Hesperia	$17^h20^m36.01^s$	−12°36′35.7″	12.23	3.288	11.11	96
110	Lydia	$11^h47^m37.18^s$	7°51′15.0″	12.57	2.922	14.97	84
125	Liberatrix	$10^h4^m39.43^s$	10°44′38.20″	13.25	2.823	10.89	80
136	Austria	$12^h49^m23.93^s$	−4°36′56.0″	12.77	2.401	5.03	50
201	Penelope	$15^h3^m2.28^s$	−8°32′41.3″	12.19	2.782	3.34	90
216	Kleopatra	$10^h53^m13.90^s$	−3°8′52.6″	12.66	3.300	14.55	108
325	Heidelberga	$12^h22^m3.87^s$	−9°0′5.6″	14.17	3.618	8.06	4

Table 3
Selected M-asteroid physical and dynamical parameters

Asteroid		Diameter (km)[a]	Albedo[a]	a (AU)[b]	e[b]	Rational period (h)[c]
16	Psyche	253.16	0.1203	2.922	0.100	4.196
69	Hesperia	138.13	0.1402	2.979	0.174	5.655
110	Lydia	86.09	0.1808	2.733	0.047	10.927
125	Liberatrix	43.58	0.2253	2.743	0.086	3.969
136	Austria	40.14	0.1459	2.287	0.023	11.5
201	Penelope	68.39	0.1604	2.678	0.140	3.747
216	Kleopatra	135.07	0.1164	2.795	0.224	5.385
325	Heidelberga	75.72	0.1068	3.206	0.128	6.737[d]

[a] Tedesco and Veeder (1992). [b] Williams (1989). [c] Lagerkvist et al. (1989). [d] Harris et al. (1992).

dependent extinction coefficients can be calculated for the sky above Mauna Kea. A local standard, typically a G-type main sequence star which is located close to the asteroid in the sky, is usually selected for each asteroid. This helps to ensure that the atmospheric conditions experienced by the asteroid and star are as similar as possible during the course of their observations.

Solar analog stars, which exhibit spectra similar to the Sun (Hardorp, 1978), are also observed. They are used in the data reduction process to eliminate any spectral features or spectral slope variations caused by the use of non-G2V local standard stars. However, non-G2V stars can be used if the ratio of the candidate star to a calibrated solar analog produces a zero-slope line. Both HD 186427 (16 Cyg B, G3V) and HD 120050 (G5III) were used as solar analogs for this work. HD 120050 has been calibrated relative to a solar analog star and exhibits a near zero-slope ratio.

2.2. Data reduction

The primary data reduction steps include removing spectral channel offsets caused by instrument flexure (which varies with telescope orientiation), calculation of wavelength-dependent extinction coefficients, division of each asteroid spectrum by the local standard star spectrum (corrected to the same airmass as the asteroid observation using the calculated extinction coefficients), and division of each solar analog spectrum by the local standard star spectrum using the same extinction correction procedure. The final step to produce an asteroid reflectance spectrum is described by the following equation:

$$\text{Asteroid/Sun} = (\text{Asteroid/Standard Star}) \times (\text{Solar Analog/Standard Star})^{-1}.$$

Data reduction is accomplished through initial processing with IRAF to collapse asteroid and stellar spectra into one-dimensional arrays of flux values. Spectrum curvature is corrected by using IRAF to trace the maximum object flux along each spectrum. Background sky removal is usually accomplished by pairing adjacent spectra and taking their difference. The background sky signal is removed from a single, unpaired spectrum by selecting a region of the background sky adjacent to the object signal and subtracting that from the object flux. These data are then imported into SpecPR, which is a PC-based one-dimensional spectral processing program created by Clark (1980) and modified by Gaffey (2003).

Channel offsets are corrected by shifting all object spectra to an arbitrary reference spectrum. Uncorrected final asteroid spectra can exhibit significant artifacts which would severely affect further data analysis (e.g., Fig. 2 of Gaffey et al., 2002). After deriving the nightly model of the Mauna Kea sky from local standard star observations, each asteroid spectrum is ratioed to the extinction-corrected local standard star spectrum. The same procedure is applied to the solar analog star.

Several permutations of the extinction coefficients are calculated (e.g., from all observations of a local standard star, from the pre-meridian and post-meridian observations, from the sets of observations bracketing a given set of as-

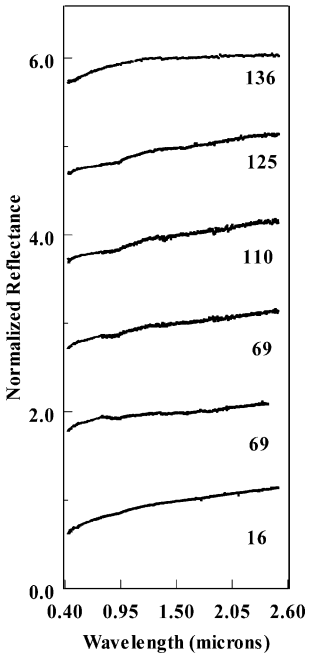

Fig. 1. The average spectra for 16 Psyche (3/22/2002), 69 Hesperia (5/3 and 4/2001), 110 Lydia (5/4/2001), 125 Liberatrix (3/23/2002), and 136 Austria (3/22/2002). Individual spectra are offset for clarity.

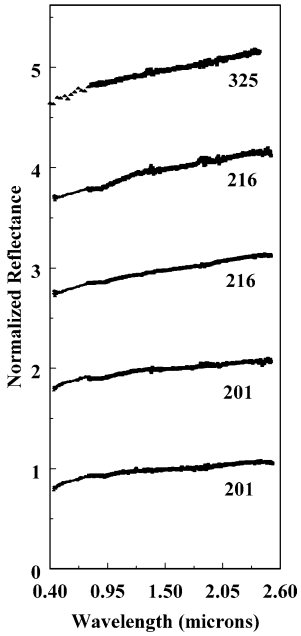

Fig. 2. The average spectra for 201 Penelope (5/2 and 3/2001), 216 Kleopatra (4/29 and 5/4/2001), and 325 Heidelberga (4/29/2001). Individual spectra are offset for clarity.

teroid observations, etc.). Although the best extinction corrections are often derived from the sets of standard star observations immediately preceding and following each set of asteroid observations, the various permutations allow evaluation of extinction corrections derived from larger sets of standard star observations over more extended periods, potentially increasing the signal-to-noise level of the resulting asteroid/star ratio.

The extinction coefficients are calculated from a minimum of twenty (and often sixty or more) observations of the local standard star. Each asteroid observation is reduced via all of the appropriate extinction coefficient permutations. The best reduction of each observation is selected from among the several permutations on the basis of how well each removes the effects of the telluric water vapor absorption features, using the profile of those features as a template to identify over-correction or under-correction. When two or more reductions are considered equally good, the reduction involving extinction coefficients derived from the largest number of standard star observations is chosen. The best resulting asteroid and solar analog spectra are then averaged to obtain an all-night average spectrum or an average spectrum for one set of observations. The final step in producing fully-reduced asteroid spectra is to apply the equation above, which involves taking the ratio of each average asteroid spectrum to the average solar analog spectrum. This produces a normalized, average reflectance spectrum that is ready for further analysis.

Figures 1 and 2 show the all-night average spectra for the eight asteroids in this paper. All of these asteroids, except for 325 Heidelberga, are combined with data from the SMASS II survey (Bus and Binzel, 2002). The SMASS II data typically extends from ~ 0.435 to ~ 0.925 μm; SpeX data in this paper begins at ~ 0.772 μm. The SMASS II data were truncated at ~ 0.77 μm and vertically offset to combine smoothly with the SpeX data. The spectrum for 325 Heidelberga is combined with data from the 24-color survey (Chapman and Gaffey, 1979).

3. Data analysis

3.1. Band centers

Six of the eight M-asteroids shown in Figs. 1 and 2 exhibit weak spectral absorption features at ~ 0.9-μm. The feature for 16 Psyche is the weakest, which appears only as an inflection superimposed on the overall spectrum as seen in Fig. 1. The features for 69 Hesperia, 110 Lydia, 125 Liberatrix, 201 Penelope, and 216 Kleopatra are stronger, but still quite weak ($\sim$ 2–3%). For five of these asteroids—16 Psyche, 69 Hesperia, 110 Lydia, 125 Liberatrix, and 216 Kleopatra—these features are present in *all* of the spectra taken over multiple nights. 201 Penelope is the only asteroid that exhibits variations in the intensity and presence of the ~ 0.9-μm feature.

A continuum-removed absorption feature is produced by taking the ratio of a straight-line continuum to the absorption feature. The end-points of the continuum (i.e., specific wavelengths) are located at maxima that bound the absorption feature. Although this type of continuum does not accurately represent the continua of real planetary objects, it is used for convenience and is the same method that has been applied to

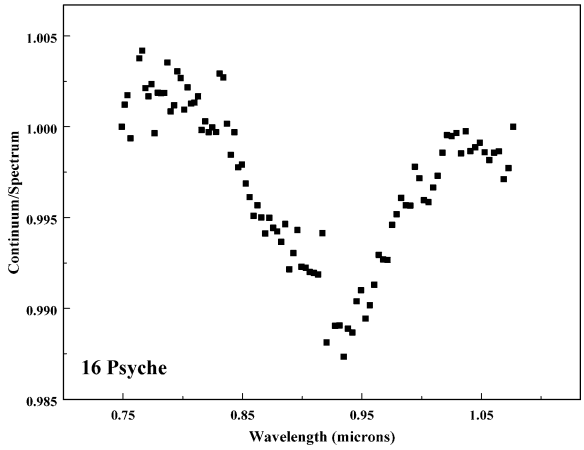

Fig. 3. 16 Psyche: Band I continuum-removed absorption feature, 3/22/2002.

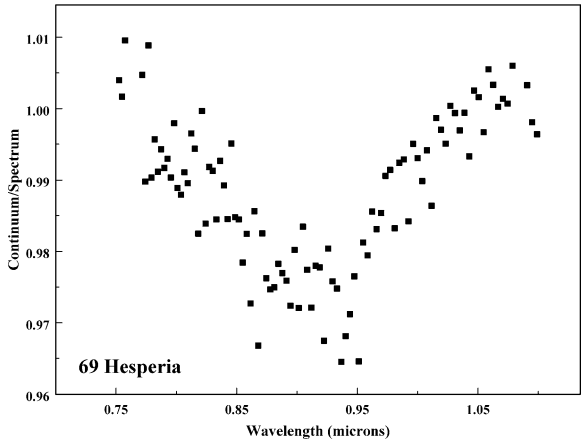

Fig. 4. 69 Hesperia: Band I continuum-removed absorption feature, 5/3/2001.

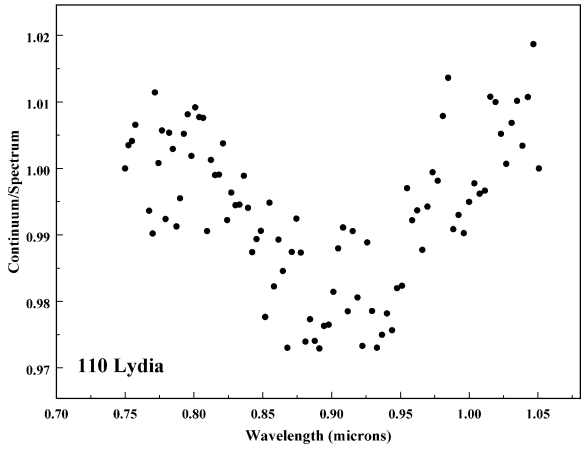

Fig. 5. 110 Lydia: Band I continuum-removed absorption feature, 5/4/2001.

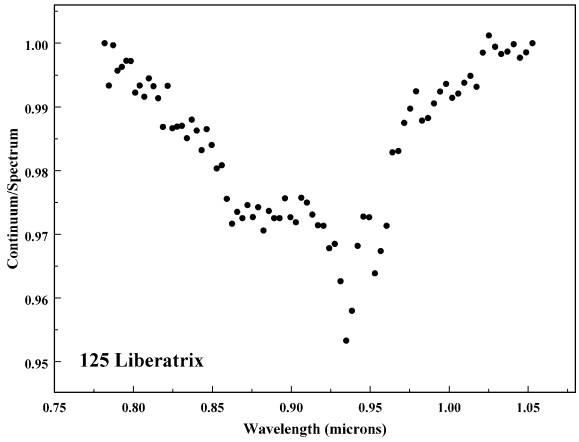

Fig. 6. 125 Liberatrix: Band I continuum-removed absorption feature, 3/23/2002.

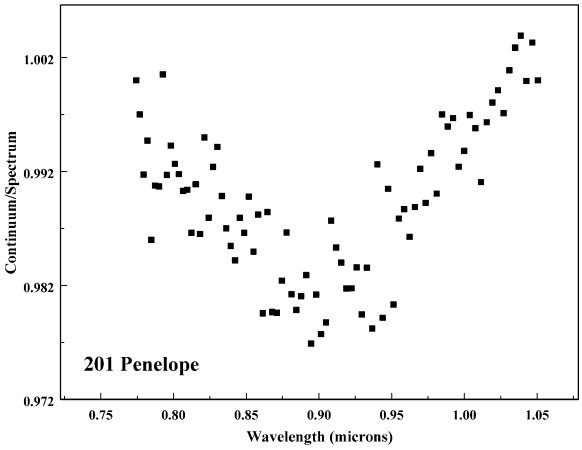

Fig. 7. 201 Penelope: Band I continuum-removed absorption feature, 5/3/2001.

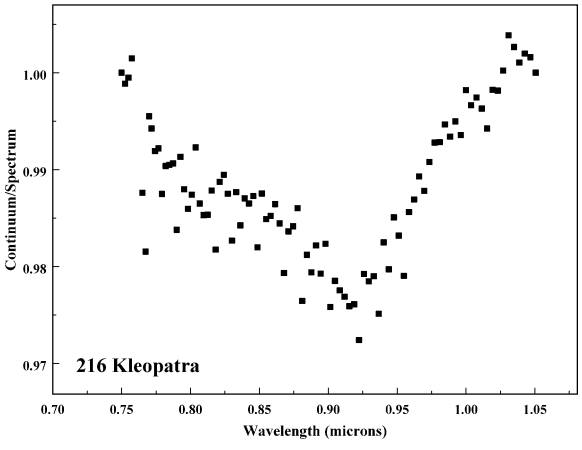

Fig. 8. 216 Kleopatra: Band I continuum-removed absorption feature, 4/29/2001.

the study of the mineralogic parameters of meteoritic spectra (Cloutis et al., 1986).

Figures 3–8 display the ∼ 0.9-μm continuum-removed absorption features for each of the six asteroids. The feature for 16 Psyche is only ∼ 1% deep, but is well-defined. The features for the other asteroids display depths of ∼ 2–3%, depending on the asteroid. Although these are weak features, they persist throughout a given night and across multiple nights. The feature in the spectra of 201 Penelope is

Table 4
Spectral and mineral chemistry data for 69 Hesperia, 110 Lydia, 201 Penelope, and 216 Kleopatra

Asteroid	Date	Set #	Band I center (μm)	Band II center (μm)	Petrology
69 Hesperia	5/2/2001	All Night	0.93	1.83	$Wo_{10}Fs_7En_{83}$
69 Hesperia	5/2/2001	1	0.92	1.80	–
69 Hesperia	5/2/2001	2	0.92	1.81	$Wo_6Fs_2En_{92}$
69 Hesperia	5/2/2001	3	0.92	1.85	$Wo_6Fs_{12}En_{82}$
69 Hesperia	5/3/2001	All Night	0.91	1.78	–
69 Hesperia	5/3/2001	1	0.90	1.71	–
69 Hesperia	5/3/2001	2	0.92	1.73	–
69 Hesperia	5/3/2001	5	0.92	1.75	–
69 Hesperia	5/3/2001	6	0.92	1.77	–
110 Lydia	5/2/2001	All Night	0.91	1.75	–
110 Lydia	5/2/2001	1	0.91	1.71	–
110 Lydia	5/2/2001	2	0.91	1.89	$Wo_3Fs_{23}En_{74}$
110 Lydia	5/2/2001	3	0.91	1.87	$Wo_3Fs_{17}En_{80}$
110 Lydia	5/3/2001	All Night	0.91	1.80	–
110 Lydia	5/3/2001	2	0.91	1.75	–
110 Lydia	5/4/2001	All Night	0.91	1.90	–
110 Lydia	5/4/2001	1	0.91	1.89	–
201 Penelope	5/2/2001	All Night	0.93	1.83	$Wo_{10}Fs_7En_{83}$
201 Penelope	5/2/2001	1	0.93	1.77	–
201 Penelope	5/2/2001	2	0.93	1.80	–
201 Penelope	5/2/2001	3	0.91	1.81	$Wo_3Fs_2En_{95}$
201 Penelope	5/2/2001	4	0.92	1.89	–
201 Penelope	5/3/2001	All Night	0.90	1.82	–
201 Penelope	5/3/2001	1	0.91	1.86	–
201 Penelope	5/3/2001	2	0.89	1.74	–
216 Kleopatra	4/29/2001	All Night	0.91	1.81	$Wo_3Fs_2En_{95}$
216 Kleopatra	4/29/2001	1	0.93	1.71	–
216 Kleopatra	4/29/2001	2	0.92	1.74	–
216 Kleopatra	4/29/2001	3	0.92	1.82	$Wo_6Fs_4En_{90}$
216 Kleopatra	4/29/2001	4	0.91	1.84	$Wo_3Fs_{10}En_{87}$
216 Kleopatra	5/4/2001	All Night	0.90	1.79	–
216 Kleopatra	5/4/2001	3	0.88	1.89	–

Mineral chemistries calculated using the calibration technique from Gaffey et al. (2002). Mineral chemistries omitted if band center data produce unrealistic petrologies (i.e., negative values) or do not converge when applying the techniques in Gaffey et al. (2002).

somewhat ephemeral, but it is still seen on both nights of observation.

Polynomial functions were then fit to the continuum-removed absorption features for each asteroid to determine their individual band centers. Tables 4 and 5 show the band centers for each asteroid observational set, as well as the band centers for each all-night average spectrum. Most of the calculated band centers range from 0.89 to 0.94 μm, although one set for 216 Kleopatra on May 4, 2001, produced a band center of 0.88 μm.

Qualitatively, several of the M-asteroids appear to have very weak (and equivocal, $< 1\%$) $\sim$ 2-μm spectral absorption features. Attempts were made to isolate these longer wavelength features and determine their band centers in the same fashion as the shorter wavelength features. The results are much less certain due to the weakness of the features and the noisier data present in this spectral region, which is caused by telluric water vapor absorptions in the $\sim$ 1.8 to $\sim$ 2.0 μm spectral region. Table 4 lists the $\sim$ 2-μm band centers for these objects. These band center estimates have large uncertainties and it is possible that these absorption bands are not detectable. However, the absence of these bands does not change the results and interpretations of this work.

Note that some of the calculated band centers are at anomalously short wavelengths ($<$ 1.8-μm). If these features are caused by the presence of pyroxenes on asteroid surfaces, as will be discussed below, then empirical calibrations suggest that the long wavelength band centers should not migrate much shorter than $\sim$ 1.80 μm (Adams, 1974; Cloutis and Gaffey, 1991). The anomalously short wavelengths (as well as the longest wavelengths) probably arise from a distortion of the weak pyroxene band by the incomplete correction of the 1.80- to 1.95-μm telluric water vapor feature. For these weak features, even a few percent over-correction or under-correction of the water vapor feature can substantially distort the 2-μm mafic silicate feature.

3.2. Atmospheric water vapor feature

Due to the weakness of the $\sim$ 0.9-μm absorption features in the asteroid spectra, one must evaluate the possibility that these may simply be due to incompletely corrected telluric water vapor features. This can be tested by comparing the band centers and band widths of the absorptions in the asteroid spectra to the telluric $\sim$ 0.9-μm water vapor absorption found in the raw spectra of a star. If the asteroid features

Table 5
Band centers and mineral chemistries for 16 Psyche and 125 Liberatrix

Asteroid		Date	Set #	Band I center (μm)	Band II center (μm)	Petrology
16	Psyche	3/22/2002	All Night	0.93	–	–
16	Psyche	3/22/2002	1	0.93	–	–
16	Psyche	3/22/2002	2	0.93	–	–
16	Psyche	3/22/2002	3	0.93	–	–
16	Psyche	3/22/2002	4	0.93	–	–
16	Psyche	3/22/2002	5	0.93	–	–
16	Psyche	3/22/2002	6	0.92	–	–
16	Psyche	3/22/2002	7	0.93	–	–
125	Liberatrix	3/23/2002	All Night	0.91	–	–
125	Liberatrix	3/23/2002	1	0.91	–	–
125	Liberatrix	3/23/2002	2	0.91	–	–
125	Liberatrix	3/23/2002	3	0.92	–	–
125	Liberatrix	3/23/2002	4	0.92	–	–
125	Liberatrix	3/23/2002	5	0.91	–	–
125	Liberatrix	3/23/2002	6	0.91	–	–
125	Liberatrix	3/23/2002	7	0.91	–	–

The Band I features for 16 Psyche are ∼ 1% deep. No Band II features are present. The lack of Band II features for the inferred pyroxenes is likely due to the weakness of the absorption features that are masked in the ∼ 2-μm region. Attempts to determine Band II centers for 125 Liberatrix result in values at anomalously short wavelengths. An asteroid "set" consists of an average of 8 to 16 spectra.

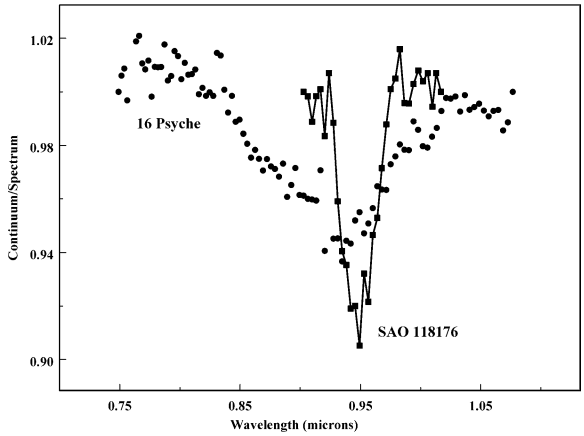

Fig. 9. Overlay of the ∼ 0.94-μm telluric water vapor feature from a 10-spectrum average of SAO 118176 and the Band I continuum-removed absorption feature for 16 Psyche. The Psyche spectrum has been exaggerated for this comparison.

are caused by telluric water vapor, then they should exhibit band centers and widths similar to those features found in any raw, uncorrected spectrum. An atmospheric water vapor feature was isolated in a 10-spectrum average for HD 88725 via the application of a straight-line continuum across the feature. The best-fit polynomial function produced a band center at 0.94 μm. Figure 9 compares this water vapor feature to a continuum-removed feature for 16 Psyche. This comparison shows that the band centers from the two spectra are not equivalent and their widths are significantly different. For 16 Psyche, as well as the other M-asteroids with absorption features, the ∼ 0.9-μm feature widths are much wider (∼ 3 to 4 times) than the telluric water vapor feature.

Based on these comparisons, the continuum-removed ∼ 0.9-μm absorption features in the spectra of the six M-asteroids are not produced by telluric water vapor. However, distortions of asteroid absorption features can occur, as can be seen by the shape of the Psyche absorption feature in Fig. 9. This shape suggests that there is a slight undercorrection (2%) of the telluric absorption which somewhat distorts the Psyche feature. The narrower telluric feature at ∼ 0.94 μm can distort a small portion of the broader asteroid ∼ 0.9-μm feature. This distortion is readily apparent when it occurs; the distorted data points are omitted before applying a polynomial fitting routine to determine band centers.

3.3. Other spectral and physical effects

Several additional factors may affect an asteroid's reflectance spectrum and any absorption features that may be present. Changing sky conditions, the presence of stellar spectral features, and space weathering are observational and physical considerations that are well known to planetary astronomers. Might any of these factors create anomalous weak absorption features in near-infrared asteroid spectra?

Changing sky conditions are unlikely to have any effect as our observational protocols require photometric conditions during asteroid observations. If the atmosphere is turbulent (but clear) and changes through the night, those changes can be accommodated through our data reduction regime. Instead of modeling the sky for an entire night, several sky models are derived over short time periods that are nearly equivalent to the all night sky model. This adjustment allows compensation for changing sky conditions that result in higher-quality asteroid spectra.

Stellar spectral absorption features are very narrow compared to the broad absorption features seen in visible- and near-infrared asteroid spectra. None of the local or solar analog stars used in this paper have shown any anomalous absorption features through the ∼ 0.8- to ∼ 2.5-μm region.

However, if features were present in the local or solar analog stars, they would usually manifest themselves during the data reduction process.

If either the local or solar analog star had an absorption feature in the near-infrared region, this would be visible when dividing the solar analog spectrum by the local standard star spectrum. If only the solar analog had the feature, the solar analog-to-local-standard ratio would show a typical negative absorption feature. If only the local standard had the feature, then the same ratio would produce an apparent emission feature that should be very noticeable. In the case where both stars have the same anomalous feature at the same wavelength position, their ratio would diminish or remove the effect of both features. If any unusual positive or negative features are seen in the spectra of a local or solar analog star, the data reduction process would be halted until the nature of this feature could be discerned.

Some aspects of asteroid space weathering are currently thought to be similar to lunar space weathering, which produces vapor-deposited nano-phase Fe^0 particles on grain rims from micrometeorite impacts or solar wind-induced sputtering (Clark et al., 2002). This type of space weathering only influences asteroid compositional studies if the mineralogically diagnostic band centers for the important mafic silicate minerals are significantly shifted to different wavelengths (Gaffey, 2001).

Asteroid space weathering effects should be subdued compared to the Moon and show lesser amounts of alteration products (Noble et al., 2004). Moroz et al. (1996) simulated space weathering effects and show that clinopyroxene, olivine, and olivine–clinopyroxene mixtures exhibit non-systematic band shifts of ±0.004 μm. Similarly, individual olivine absorption bands show non-systematic variations of ∼ 0.025 μm or less (Hiroi and Sasaki, 2001). This evidence suggests that the band variations are minimal and not an important consideration when deriving quantitative mineralogical information from asteroid near-infrared reflectance spectra. Models of space weathering also indicate that these processes should *not* produce additional absorption features in the spectra of planetary bodies composed of meteorite-like assemblages.

3.4. 136 Austria and 325 Heidelberga

These asteroids do not exhibit any absorption features discernible beyond the scatter of their data. Data for 136 Austria has been combined with SMASS II data (Bus and Binzel, 2002). The Austria spectrum in Fig. 1 increases in reflectance until ∼ 1.3 μm and then rolls over to produce an almost horizontal spectrum at longer wavelengths. The spectrum of 325 Heidelberga is shown combined with 24-color survey data (Chapman and Gaffey, 1979) in Fig. 2. The IRTF spectrum of 325 Heidelberga is almost linear with reflectance increasing with wavelength.

3.5. Mineral chemistries

The absorption features present in the ∼ 0.9-μm spectral region for 16 Psyche, 69 Hesperia, 110 Lydia, 125 Liberatrix, 201 Penelope, and 216 Kleopatra are attributed to the presence of low-Fe, low-Ca orthopyroxene minerals. The band center data from Table 3 were applied to the mineral chemistry calibration in Gaffey et al. (2002) to calculate the mineral chemistries for each asteroid. Only those band center data that passed two tests were used to determine pyroxene mineral chemistries. First, the band center data for each observational set had to possess plausible values that allowed the data to be plotted on the pyroxene determinative curve of Adams (1974), which was later modified by Cloutis and Gaffey (1991). Although olivine-rich mixtures of olivine and pyroxene can cause band center data to plot above the pyroxene curve (Adams, 1974), no published work suggests that olivine–pyroxene mineral mixtures can produce data that plot below the pyroxene curve.

The calculation of plausible mineral chemistries in Gaffey et al. (2002) constitutes the second test. If the band center data produced unrealistic results (i.e., negative Wo, Fs, or En abundances), then the data were not used.

As mentioned above, many of the long-wavelength absorptions produce seemingly anomalous band centers in the 1.70- to 1.80-μm spectral region. The original data in Adams (1974) suggests that the short wavelength limits for calibrated pyroxene data are ∼ 0.90 and ∼ 1.80 μm. The apparently anomalous band center values are attributed to the effect of incomplete correction of telluric water vapor features on these very weak silicate features. The common presence of discernible absorption features in the ∼ 0.9-μm region but not in the ∼ 1.8- to 1.9-μm region is consistent with the relative weakness of the longer wavelength absorptions in the spectra of most pyroxene assemblages. The abundances of these mineral phases on the asteroid surfaces are probably minor and may be somewhat masked by other non-absorbing phases.

Table 4 lists the derived mineral chemistries for those asteroid observational sets that passed the above tests. In all cases, the Wo component is less than 10% and the Fs component is less than 25%—although most calculations show the Fs component to be less than 10%. This information suggests that these are low-Fe, low-Ca orthopyroxenes that are present on the M-asteroid surfaces. The band centers for 69 Hesperia, 110 Lydia, 201 Penelope, and 216 Kleopatra are plotted on the pyroxene determinative curve in Fig. 10. Note that all four asteroids plot in the lower left region of the diagram corresponding to orthopyroxene minerals.

For 16 Psyche and 125 Liberatrix, band center data are shown in Table 5. 16 Psyche does not exhibit any discernible ∼ 2-μm features and attempts to isolate the long-wavelength absorptions in the spectra of 125 Liberatrix produced anomalous results. 136 Austria is featureless in the 0.4- to 2.5-μm spectral region; 325 Heidelberga does not show any features above the noise level. However, further high-quality obser-

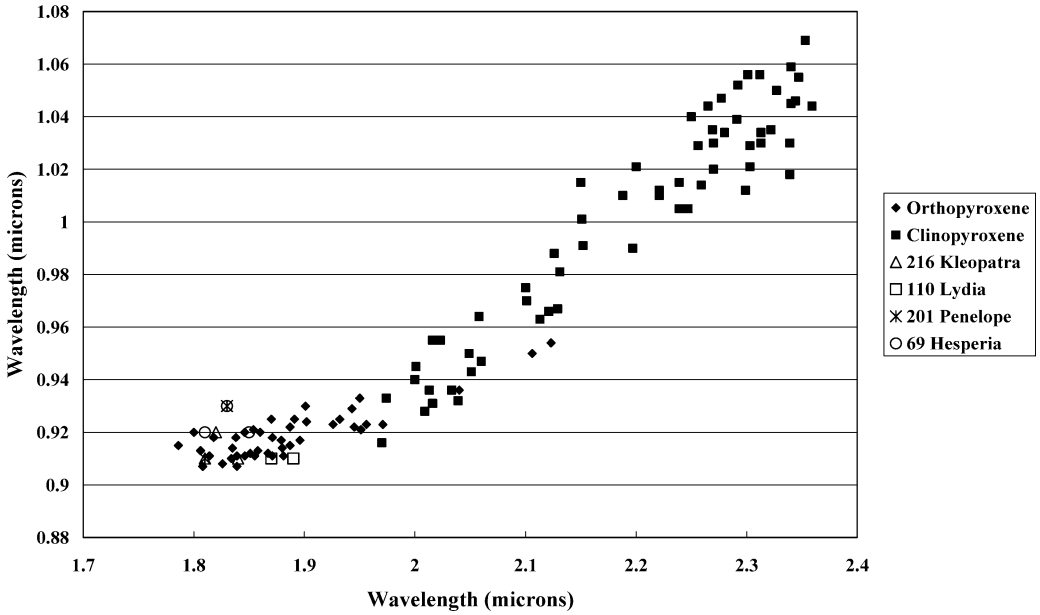

Fig. 10. Pyroxene determinative curve with data from 69 Hesperia, 110 Lydia, 201 Penelope, and 216 Kleopatra.

vations of 325 Heidelberga may confirm the presence of a possible very weak ∼ 0.9-μm feature.

3.6. Rotational coverage

69 Hesperia, 110 Lydia, 201 Penelope, and 216 Kleopatra were observed through ∼ 75% of their respective rotation periods, while 16 Psyche and 125 Liberatrix were observed through at least one full rotation. All of these asteroids, with the exception of 201 Penelope, exhibit ∼ 0.9-μm spectral absorption features through all observations. 201 Penelope is unique because its feature varies in strength and presence over the two nights when the asteroid was observed. Table 6 shows a rotational analysis of each asteroid during its observations. The features on 201 Penelope vary from being clearly present to being weak, indeterminate, or absent. This suggests that the pyroxene abundance across Penelope's surface varies somewhat with rotation or there are regions with Fe-free pyroxene (enstatite).

4. Interpretations

Four scenarios can potentially account for the presence of low-Fe, low-Ca orthopyroxenes on the surfaces of M-asteroids. These include: (1) the pyroxenes represent residual mantle material on (or silicate inclusions within) the partial or intact cores of differentiated asteroid parent bodies, (2) the pyroxenes represent the products of a high-temperature smelting reaction between carbon and olivine in the original parent assemblage, (3) the asteroids are analogs to the primitive, reduced, metal-rich Bencubbinite meteorites, and (4) the pyroxenes are included in asteroidal/meteoritic debris accreted onto the metallic surfaces of these asteroids.

4.1. Mantle/core option

The combination of relatively weak (∼ 1–3%) low-Fe, low-Ca orthopyroxene absorption features superimposed on near-infrared asteroid spectra that exhibit variably increasing (i.e., reddened) slopes suggest that the orthopyroxenes are remnant mantle material on partial or intact metallic cores from differentiated and disrupted parent bodies. Asteroids composed primarily of NiFe metal with accessory mantle pyroxene will display spectra like that for the six M-asteroids with the ∼ 0.9-μm absorption feature. Similarly, asteroids analogous to the silicate-bearing iron meteorite types (e.g., IAB, IIE, IIICD, and IVA irons) would also exhibit mafic silicate features. The silicates within these iron meteorites have typically low iron abundances (IAB = 2.55 to 5.6 wt%; IIE = 9.1 to 14.8 wt%; IVA = $Fs_{13.6\text{ to }15.0}$: Mittlefehldt et al., 1998). All six asteroids with the orthopyroxene feature display increasing slopes at longer wavelength, but to varying degrees. 16 Psyche and 216 Kleopatra exhibit the steepest slopes while 201 Penelope has the flattest slope among these asteroids. Gaffey (1976) showed that NiFe meteorite spectra can show a variety of slopes ranging from positive to zero to negative at longer wavelengths.

In addition, the nature of the terrestrial meteorite collection suggests the abundant presence of metallic cores in the asteroid belt. Wasson (1990) suggests that 40–55 meteorite parent bodies are the sources of an equivalent number of structurally and compositionally unique iron meteorites in the terrestrial collection. Keil (2000) suggests that ∼ 85 parent bodies are required to account for the chemical diversity of the iron meteorites in the terrestrial collection. In

Table 6
Analysis of rotational coverage of 69 Hesperia, 110 Lydia, 201 Penelope, and 216 Kleopatra

Date	Time (UT)	Set #	1-μm feature (absent/present)	Surface location (0° to 360°)
16 Psyche				
3/22/2002	646	1	Present	0
3/22/2002	725	2	Present	56
3/22/2002	751	3	Present	93
3/22/2002	821	4	Present	136
3/22/2002	901	5	Present	193
3/22/2002	1007	6	Present	287
3/22/2002	1133	7	Present	50
69 Hesperia				
5/2/2001	1336	1	Present	0
5/2/2001	1407	2	Present	33
5/2/2001	1445	3	Present	73
5/3/2001	1126	1	Present	310
5/3/2001	1212	2	Present	359
5/3/2001	1251	3	Present	40
5/3/2001	1337	4	Present	89
5/3/2001	1421	5	Present	136
5/3/2001	1454	6	Present	171
5/4/2001	1329	1	Present	169
5/4/2001	1425	2	Present	228
110 Lydia				
5/2/2001	624	1	Present	0
5/2/2001	754	2	Present	49
5/2/2001	920	3	Present	97
5/3/2001	550	1	Present	52
5/3/2001	700	2	Present	90
5/3/2001	824	3	Present	137
5/3/2001	959	4	Present	189
5/4/2001	915	1	Present	235
5/4/2001	1030	2	Present	277
125 Liberatrix				
3/23/2002	518	1	Present	0
3/23/2002	533	2	Present	23
3/23/2002	614	3	Present	85
3/23/2002	653	4	Present	144
3/23/2002	724	5	Present	190
3/23/2002	800	6	Present	245
3/23/2002	834	7	Present	296
3/23/2002	912	8	Present	354
201 Penelope				
5/2/2001	1038	1	Weak	0
5/2/2001	1127	2	Present	78
5/2/2001	1207	3	Present	143
5/2/2001	1237	4	Present	191
5/3/2001	900	1	Weak	349
5/3/2001	939	2	Present	51
5/3/2001	1038	3	Indeterminate	146
5/3/2001	1146	4	Absent/Weak	255
5/3/2001	1232	5	Absent/Weak	328
5/3/2001	1306	6	Absent/Weak	23
216 Kleopatra				
4/29/2001	600	1	Present	0
4/29/2001	711	2	Present	55
4/29/2001	756	3	Present	129
4/29/2001	839	4	Present	177
5/2/2001	703	1	Present	204
5/2/2001	829	2	Present	299
5/4/2001	619	1	Present	319
5/4/2001	807	2	Present	79
5/4/2001	848	3	Present	125

that same work, Keil (2000) conducted a macroscopic analysis of the meteorite collection and showed that ∼ 80% of the meteorite types currently present have experienced melting temperatures (∼ 950 °C or higher) and the remaining ∼ 20% have experienced significant alteration at lower temperatures. This strongly implies an early inner Solar System heating event that substantially altered many asteroid parent bodies. Thus, it would not be surprising to find many core remnants within the asteroid belt.

4.2. Parent body smelting option

Most meteorite types contain some amount of carbon (Brett and Sato, 1984), with the carbonaceous chondrites and the ureilites (olivine-rich achondrites) having the highest relative proportions of carbon compounds. A scenario can be envisioned where an asteroid parent body consists of a few percent carbon and a relatively large amount of iron-bearing olivine. If the parent body were to experience temperatures of ⩾ 850 °C, then the carbon will react with the fayalite (bivalent iron, Fe^{2+}) component of the olivine to produce iron-poor pyroxene and metallic iron. If sufficient carbon is present as a reducing agent, the final products would be iron-free pyroxene (enstatite), metallic iron, and possibly silica. This process is invoked to produce the metallic iron-bearing reaction rims on olivine grains in some ureilites (Walker and Grove, 1993). The reactions for this process are shown in the following equation:

$$(Fe,Mg)_2SiO_4\ (s) + C\ (s) \rightarrow MgSiO_3\ (s) + Fe\ (s) + CO \quad \text{or} \quad CO_2\ (g) \pm SiO_2\ (s).$$

This smelting-type reaction would chemically reduce the fayalite to enstatite, solid Fe, and CO or CO_2 gas. Depending upon the limiting reactant, the reaction will proceed until the carbon or the fayalite component of the olivine is depleted, assuming sufficient temperatures are maintained to promote the reaction. If insufficient reducing agent is present, the final assemblage will be composed of a mixture of iron-poor olivine and pyroxene plus iron metal. This reaction also has a pressure dependency (Walker and Grove, 1993) and will not proceed within parent bodies with pressures (and sizes) sufficient to halt the reaction. Although smelting is most commonly invoked as a mechanism for ureilite petrogenesis (Walker and Grove, 1993), it can be applied to the six M-asteroids without invoking any association between these asteroids and the ureilites.

The difficulty with this explanation is that the presence of iron-bearing (albeit low iron) pyroxenes on these M-asteroid surfaces would imply incomplete reduction of the bivalent iron species and the presence of a residual fayalite (olivine) component. The short-wavelengths of the band centers and the narrowness of the features suggest that olivine is a relatively minor mafic mineral component. Attempts were made to calculate band area ratios to quantify the relative amount of olivine (Cloutis et al., 1986), but this was unsuccessful due to the extreme weakness and variability of the long-wavelength pyroxene bands.

4.3. Bencubbinite option

In contrast to the previous two high-temperature scenarios, the Bencubbinite (CB) chondrites could serve as possible analogs for the six M-asteroids with orthopyroxene spectral features. Bencubbinites are very chemically reduced, primitive, brecciated meteorites consisting of ∼ 40 (30–60) vol% silicate clasts and ∼ 60 (40–70) vol% metal (Weisberg et al., 1990, 2001; Rubin et al., 2003). The silicate components are all very Fe-poor with 1.4–4.1% fayalite in the olivine, ∼ 2.3% ferrosilite in low-Ca pyroxene, and ∼ 2.0% ferrosilite in high-Ca pyroxene (Weisberg et al., 1990, 2001).

Difficulties with this scenario may include the proportion of olivine-to-pyroxene in the silicate portions of the meteorite and the postulated formation scenarios. Weisberg et al. (1990) used an automated electron microprobe point counting technique to determine an overall silicate fraction in Bencubbinite meteorites of 40% olivine and 47% pyroxene, by volume. For an olivine/pyroxene mixture with this ratio, calibrations by Cloutis et al. (1986) require a band center of at least ∼ 0.925 μm. 16 Psyche and possibly 69 Hesperia and 201 Penelope would meet this requirement, but the remaining M-asteroids that display spectral features would not. However, normative calculations from bulk silicate compositions (Weisberg et al., 2001) indicate a substantially lower olivine abundance (∼ 13–26%) as does the low iron content of these otherwise chondritic silicates, so this may not present a problem for a Bencubbinite-like interpretation.

However, the formation scenarios for the Bencubbinites do present a significant problem for such an interpretation. The composition of the metal phases are interpreted to indicate condensation either directly from the solar nebula or from an impact generated vapor plume (Newson and Drake, 1979; Petaev et al., 2001; Weisberg et al., 2001; Campbell et al., 2002; Rubin et al., 2003). If the impact origin (which is currently preferred) is correct, then the six M-asteroids are unlikely to be similar to the Bencubbinites because spectral features are seen consistently across ∼ 100% of the observed surfaces of each asteroid (except 201 Penelope). Impact-generated deposits are usually thought of as a localized phenomena and it is difficult to envision this process occurring across most of an asteroid's surface. The nebular condensation formation scenario would make this option more favorable as the meteorite is formed directly from nebular condensates that are later impact shattered, re-accreted, and cemented with minor impact melting (Weisberg et al., 1990).

4.4. Accretion of asteroidal silicate debris onto metallic surfaces

This scenario envisions the accretion of silicate-dominated impact debris produced by impacts onto or collisions between anhydrous silicate-dominated asteroids (e.g., S-, V-, R-types, etc.) onto the metallic surfaces of these M-asteroids. The accreted material would need to consist pri-

marily of silicates dominated by low-Fe, low-Ca orthopyroxenes. Since the number of moderately reduced meteorites (e.g., CB, CH, K, F chondrites, etc.) in the terrestrial collection is small, it seems unlikely that only low-Fe, low-Ca orthopyroxenes would be accreted onto the surfaces of these asteroids. The ejecta from impacts and collisions across the asteroid belt should include substantial components of more oxidized silicates (more iron-rich olivines and pyroxenes) from S-, V-, R-, and A-type asteroids. Accretion of this more typical debris onto metallic surfaces would cause the band centers in asteroid near-infrared spectra to be observed at longer wavelengths than seen on the M-asteroids studied here.

5. Results for individual asteroids

5.1. 216 Kleopatra

This asteroid was observed on April 29, May 2, and May 4, 2001. A total of 115 spectra were obtained; the last set of seven spectra on April 29 was discarded due to a large amount of scatter in the data, which resulted from deteriorating sky conditions toward the end of that observing session. All spectra display the ~ 0.9-μm absorption feature through all observational sets and on all three nights. The mean Band I center is 0.91 μm, with a range from 0.88 to 0.93 μm and a band depth of $\sim 2\%$ that varies little in intensity. The mean Band II center is 1.80 μm, which ranges from 1.79 to 1.86 μm. These features are very weak ($< 1\%$). The average orthopyroxene mineral chemistry for 216 Kleopatra, based on the all night average spectrum, is $Wo_3Fs_2En_{95}$.

216 Kleopatra has been observed by Chapman and Gaffey (1979), Zellner et al. (1985), Mitchell et al. (1995), Bus (1999), Ostro et al. (2000), Rivkin et al. (2000), and Bus and Binzel (2002). Our representative spectrum in Fig. 2 is combined with data from Bus and Binzel (2002) to provide wavelength coverage from ~ 0.5 to ~ 2.5 μm. Previous radar observations by Mitchell et al. (1995) and Ostro et al. (2000) reveal Kleopatra as an oddly-shaped asteroid with the highest radar albedo of any asteroid thus far observed (0.44 ± 0.15 and 0.70, respectively). Rivkin et al. (2000) classify Kleopatra as not hydrated.

The accumulated observational data for 216 Kleopatra at near-infrared and radar wavelengths strongly suggests this object is a metallic core fragment (or rubble pile) with a minor surface component of low-Fe, low-Ca orthopyroxene-dominated mantle material. High radar albedos strongly indicate a significant metal component; few other plausible Solar System materials exist to complicate this interpretation. Based on an empirical relationship between reflection coefficient (i.e., radar albedo) and density (Ostro et al., 1985), 216 Kleopatra has an estimated surface density of 6.92 g/cm^3 based on its derived radar albedo of 0.7 (Ostro et al., 2000). The odd shape of the asteroid suggests the presence of significant macro-porosity. The high radar albedo and high surface density strongly suggest that Kleopatra's surface material is dominated by a metallic component. The reddened slope at near-infrared wavelengths seen in our spectra also supports this interpretation. The ubiquity of the spectral feature suggests that orthopyroxene is present on much of Kleopatra's surface; there may also be a small olivine component that is not spectrally detectable.

Kleopatra's parent body is suggested to have formed in relatively chemically reducing conditions in the solar nebula. The oxidation state is likely to be less than that of the H and about equivalent to the K, F, or CB chondrites. The parent body experienced an early Solar System heating event (Herbert, 1989; Herbert et al., 1991; Grimm and McSween, 1993), which caused the object to melt, chemically segregate, and develop a core, mantle, and potentially a crust. A later impact(s) disrupted much of the parent body, which re-accreted into the dog bone (contact binary?) shape that is seen today.

5.2. 16 Psyche

This asteroid was observed on March 22, 2002 over slightly more than one full rotation period. A total of 120 spectra were obtained; 118 which are used. Psyche's ~ 0.9-μm absorption feature is persistent in all spectra and averages $\sim 1\%$ in band depth. The band center average is 0.93 μm.

Psyche has also been observed by Chapman and Gaffey (1979), Ostro et al. (1985), Zellner et al. (1985), Bell et al. (1988), Jones et al. (1990), Rivkin et al. (1995), Bus (1999), Rivkin et al. (2000), and Bus and Binzel (2002). Ostro et al. (1985) derived a radar albedo of 0.29 ± 0.11 for Psyche, which was later revised to 0.32 ± 0.12 by Magri et al. (1999).

Psyche's surface density is estimated to be 3.75 g/cm^3 based on the work of Ostro et al. (1985) and Magri et al. (1999). This density value also suggests significant porosity in the top layer (~ 1 m or less) of Psyche's surface. Rivkin et al. (2000) classify Psyche as not hydrated.

The same arguments as applied to Kleopatra are applied here to suggest that Psyche is a metallic core with residual low-Fe, low-Ca orthopyroxene mantle material that is present across the asteroid. In this case, Psyche may be an intact core as it is rather large with a diameter of ~ 250 km (Table 3). Ostro et al. (1985) prefer the metallic interpretation for 16 Psyche over the enstatite chondrite interpretation based on arguments against very low porosities for enstatite chondrites. The presence of the mafic silicate feature in the Psyche spectrum indicates an iron-bearing, albeit iron-poor, pyroxene, which is inconsistent with an enstatite chondrite assemblage.

Lupishko and Belskaya (1989) suggest that several M-asteroids, including 16 Psyche, have surface silicate minerals based on polarimetric and photometric evidence. Our observations confirm their general suggestion, but differ in the specific nature of the silicates.

5.3. 69 Hesperia

Ninety-six spectra were obtained of 69 Hesperia over three nights on May 2, 3, and 4, 2001. Observations through ∼ 75% of a full rotation show a persistent ∼ 0.9-μm absorption feature that appears in all spectra. Band intensity does not vary significantly and averages ∼ 3%. The average Band I and Band II centers are 0.92 and 1.78 μm, respectively. The average orthopyroxene chemistry, based on the all night average spectrum for May 2, 2001, is $Wo_{10}Fs_7En_{83}$.

69 Hesperia has been observed by Chapman and Gaffey (1979), Zellner et al. (1985), Bell et al. (1988), Clark et al. (1995), Bus (1999), and Bus and Binzel (2002). Spectra from Bell et al. (1988) show a broad, spinel-like absorption feature longward of ∼ 1.4 μm; however, Clark et al. (1995) show no evidence of such a feature. Our observations support the work of Clark et al. (1995), but there is still the possibility that the ∼ 25% surface area not covered in this work may contain the feature seen by Bell et al. (1988).

No radar data or 3-μm data have yet been reported for 69 Hesperia. Although these supporting observations are not yet available, we interpret 69 Hesperia to be similar to 16 Psyche and 216 Kleopatra. The presence of low-Fe, low-Ca orthopyroxenes strongly suggests a chemically reducing environment for this object and, by analogy with the previous asteroids, represents a partial or intact metallic core with surface orthopyroxenes. Our work supports the results of Lupishko and Belskaya (1989), who use polarimetric and photometric evidence to suggest that 69 Hesperia has a significant surface silicate component.

5.4. 110 Lydia

This asteroid was observed on May 2, 3, and 4, 2001. The ∼ 0.9-μm absorption feature is present in all of the 84 spectra obtained of the asteroid. Observations covered ∼ 75% of the surface of the asteroid. The average Band I and II centers are 0.91 μm and 1.82 μm, respectively. Band I values average ∼ 0.91 μm and Band II values range from 1.71 to 1.90 μm. The average pyroxene chemistry for 110 Lydia is $Wo_3Fs_{17–23}En_{74–80}$. As with the other asteroids, this data indicates that Lydia's surface includes minor amounts of low-Fe, low-Ca orthopyroxene on all faces of the asteroid that were observed. The presence of silicates is supported by the polarimetric and photometric evidence of Lupishko and Belskaya (1989).

110 Lydia has also been observed by Chapman and Gaffey (1979), Zellner et al. (1985), Bus (1999), Rivkin et al. (2000), and Bus and Binzel (2002). No radar data yet exists for Lydia.

Again, by analogy, we interpret 110 Lydia to be similar to the asteroids previously discussed. This interpretation conflicts with the interpretation from Rivkin et al. (2000), who suggest that 110 Lydia has a surface consisting of phyllosilicate minerals. This interpretation is based on the presence of a 3-μm spectral absorption feature in the asteroid's spectra. These interpretations appear irreconcilable because of the vastly differing oxidation states between the reduced assemblage indicated by our data and the oxidized assemblage implied by a hydrated assemblage. However, the actual water content indicated by the 3-μm water-of-hydration feature in Lydia is only 0.14–0.27 wt% (Rivkin et al., 2000).

5.5. 201 Penelope

This asteroid was observed on May 2 and 3, 2001. Ninety spectra were obtained over ∼ 75% of one full rotation period. The ∼ 0.9-μm absorption feature is present on both nights, but the feature weakens and disappears with rotation. The average Band I and Band II centers are 0.92 and 1.82 μm, respectively. These band centers range from 0.89 to 0.93 μm and from 1.76 to 1.89 μm. The average orthopyroxene chemistry is $Wo_{3–10}Fs_{2–7}En_{83–95}$. The latter values, as with all asteroids where ∼ 1.9-μm band center determinations were attempted, suffer from uncertainty due to the extreme weakness of the features and increased scatter in the data. Again, by analogy, Penelope is interpreted to be a partial or intact metallic core with minor, variable abundances of low-Fe, low-Ca orthopyroxenes.

201 Penelope has also been observed by Zellner et al. (1985), Clark et al. (1995), Bus (1999), Rivkin et al. (2000), and Bus and Binzel (2002). As with 110 Lydia, Rivkin et al. (2000) suggest that Penelope's surface consists of abundant phyllosilicate minerals due to an absorption in the 3-μm region. The interpretational conflict here is similar to that for 110 Lydia and may simply be that the small amount of water inferred for Penelope (0.13–0.15 wt%—Rivkin et al., 2000) does not imply phyllosilicates.

5.6. 125 Liberatrix

This asteroid was observed over essentially one full rotation period on the night of March 23, 2002. The ∼ 0.9-μm absorption feature persists in all 80 spectra with little change in band intensity. The Band I center average is 0.91 μm, with a range from 0.90 to 0.92 μm. No mineral chemistry calculations were made due to the lack of reliable ∼ 1.9-μm features. Due to its spectral similarity to previous asteroids, we suggest that 125 Liberatrix is also most probably a disrupted or intact metallic core with widespread, but minor, surface orthopyroxenes.

125 Liberatrix has also been observed by Zellner et al. (1985), Clark et al. (1995), Bus (1999), Rivkin et al. (2000), and Bus and Binzel (2002). Rivkin et al. (2000) do not consider Liberatrix to be hydrated.

5.7. 136 Austria

Fifty spectra of this asteroid were obtained on March 22, 2002. The spectra are featureless at all wavelengths with increasing reflectance at shorter wavelengths that decreases, rolls over, and becomes almost horizontal at ∼ 1.3 μm.

About 36% rotational coverage was obtained for this asteroid. Clark et al. (1995) suggest that 136 Austria has a significant ~ 1-μm absorption feature. Although not seen in our spectra, it may be present on surfaces of the asteroid that we have not yet observed.

The interpretation of the spectrum of 136 Austria is less constrained than the previous asteroids due to the lack of absorption features in the near-infrared. Both iron meteorites and enstatite chondrites are potential analogs as both meteorite types can exhibit spectra similar to the spectrum of 136 Austria (Gaffey, 1976). Rivkin et al. (2000) detected a weak water-of-hydration feature for 136 Austria, but are unsure if this asteroid is hydrated due to the weakness of the detected absorption feature.

5.8. 325 Heidelberga

Only four spectra of this asteroid were obtained on April 29, 2001. As shown in Fig. 2, Heidelberga's spectrum increases almost linearly with reflectance with no apparent absorption features within the noise of the data. When examining the ~ 0.9-μm region closely, it is possible that a 1–2% feature may exist. Future high signal-to-noise ratio observations should be able to determine whether a feature actually exists in this wavelength region. The interpretations for 325 Heidelberga are currently similar to those for 136 Austria; both enstatite chondrites and nickel-iron meteorites are viable candidates for this asteroid's spectrum.

6. Discussion

As mentioned in the introduction, three general interpretations were originally devised to account for the spectra of the M-asteroids. The NiFe metal and enstatite chondrite interpretations were suggested to account for the featureless near-infrared asteroid spectra that are similar to enstatite chondrite and iron meteorite spectra (Chapman and Salisbury, 1973; Gaffey and McCord, 1979). However, the discovery of repeatable and consistent ~ 0.9-μm features on six M-asteroids eliminates the enstatite chondrite option for those asteroids. Enstatite pyroxenes within enstatite chondrites are very low in Fe (Brearley and Jones, 1998, and references therein) and unweathered (rust-free) samples of these meteorite types do not exhibit any near-infrared spectral absorption features (Gaffey, 1976). Concurrently, the presence of near-infrared spectral absorptions due to orthopyroxenes on M-asteroid surfaces suggests that NiFe metal, as a *sole* constituent, also cannot remain a viable alternative. This new constraint suggests the need for more sophisticated interpretations that will more readily explain what is likely to be a very diverse and complicated situation, geologically, for each asteroid within the asteroid belt. Interpretations using terrestrial meteorite spectra as potential analogs are a good way to start, but it is likely that interpretations will have to evolve to anticipate the existence of asteroids that do not have representative samples in the terrestrial meteorite collection.

Within the last few years, a vigorous debate has ensued concerning the existence and nature of the 3-μm absorption features that have been reported for some asteroids by Rivkin et al. (1995), Rivkin et al. (2000), and Rivkin et al. (2002). However, these are not the first authors to report 3-μm features in asteroid spectra. Feierberg et al. (1981), Lebofsky et al. (1981), and Eaton et al. (1983) reported 3-μm features in the spectra of 1 Ceres. Feierberg et al. (1981), Eaton et al. (1983), and Larson et al. (1983) also reported weaker 3-μm absorptions for 2 Pallas. Additionally, Jones et al. (1990) reported 3-μm absorptions for 1 Ceres, 2 Pallas, and 24 other asteroids—including the M-Asteroids 55 Pandora and 92 Undina.

Much of the debate has centered on the M-asteroids because many workers presume that these are metallic or enstatite chondrite-like asteroids. The suggestion of phyllosilicate minerals on M-asteroid surfaces is unexpected and confirmation of this for many M-asteroids would dramatically alter their chemical and thermal interpretations. Asteroids within a given taxonomic group will probably exhibit a significant amount of mineralogic and geologic diversity (Gaffey et al., 1993) and the discovery of mineralogically diverse asteroids within a taxonomic group should not be a major surprise, especially for a type defined on such non-diagnostic spectral parameters as the M-class.

Another interesting result of M-asteroid investigations at different wavelength regions is the divergent interpretations for 110 Lydia and 201 Penelope. While Rivkin et al. (2000) suggests the presence of surface phyllosilicates (with unknown abundance and distribution), this work suggests something very different. The interpretations of Rivkin et al. (2000) suggest a very oxidizing asteroid parent body environment. This is thought to result from parent bodies that accreted with abundant internal ice that was subsequently melted by a mild thermal event. The liquid water then reacted with mafic minerals to produce phyllosilicate minerals. The aqueous alteration of pyroxene- and olivine-group minerals leads to the formation of serpentine-group minerals, which are abundant within CI- and CM-type meteorites (see Brearley and Jones, 1998 for a review).

In contrast, this work suggests a relatively reducing chemical environment that would preclude the presence of much, if any, original ice within the Lydia and Penelope parent bodies. The pyroxene Fe content is significantly below the values for all chondrite types except for the enstatite chondrites which were ruled out previously (McSween et al., 1991). Whether due to formation in nebular regions of low oxygen fugacity or the sequestration of Fe into metallic cores following differentiation, it would be difficult to reconcile the widespread presence of phyllosilicates with low-Fe orthopyroxenes that are present across the surfaces of Lydia and Penelope. The only plausible scenario for the presence of oxidized and hydrated phyllosilicate assemblages on a surface dominated by relatively reduced anhydrous orthopy-

roxene assemblages is through collisional addition of the former assemblage.

The almost uniform distribution of low-Fe orthopyroxenes across the surfaces of six of the eight M-asteroids in this paper suggests that these are indigenous low-Fe orthopyroxenes that derive from the original parent body. Collisional low-Fe pyroxene debris across the entire surface of these asteroids seems unlikely, as mentioned previously. The unlikely co-existence of both low-Fe orthopyroxenes and phyllosilicates on the surfaces of 110 Lydia and 201 Penelope, which is implied if this work and the work of Rivkin et al. (2000) are correct, would then suggest that the phyllosilicates are collisional debris that should not be considered as part of the asteroid's initial composition.

7. Conclusions

The M-Asteroids 16 Psyche, 69 Hesperia, 110 Lydia, 125 Liberatrix, 201 Penelope, and 216 Kleopatra exhibit verifiable and repeatable absorption features in the $\sim$ 0.9-μm region of the spectrum. Qualitative features are present in the $\sim$ 2-μm region for some of these asteroids, but not for others. Band I centers for all six asteroids range from $\sim$ 0.89 to $\sim$ 0.94 μm; Band II centers, although extremely weak and often with much uncertainty, exhibit band centers in the $\sim$ 1.75- to $\sim$ 1.90-μm region. These band centers correspond to the presence of low-Fe, low-Ca orthopyroxenes that are consistently present across these asteroids' surfaces. Four interpretations have been suggested, with the leading candidate considering these asteroids as partial or intact differentiated cores that have retained a minor portion of their mantles. Their parent bodies accreted from moderately reduced nebular material which was subsequently strongly heated and underwent magmatic differentiation. The presence of relatively reducing redox conditions in the orthopyroxenes offer the hope that similar detections in other asteroids will allow the oxidation state of the formation locations of their parent bodies in the asteroid belt to be estimated. Investigation of a representative population of bodies should allow the chemical and thermal history of the main asteroid belt to be significantly constrained.

The reflectance spectra for 136 Austria and 325 Heidelberga do not exhibit absorption features in the $\sim$ 0.4- to $\sim$ 2.5-μm region, although their spectra look very different. Their compositions are not well-constrained; both asteroids' spectra are consistent with a NiFe metal and enstatite-chondrite-like composition.

Differing interpretations in the 0.8- to 2.5-μm region and the 3-μm region suggests the need for the asteroid community to collaborate to resolve these issues. Several alternative interpretations have been offered to explain 3-μm features that are compatible with the detection of weak pyroxene absorption features. It is probable that conflicting interpretations, as described here, will happen again. Creative techniques must be found that will allow the diagnostic identification of phyllosilicate minerals on asteroid surfaces that will more strongly constrain the number of CI/CM-meteorite-like asteroids that exist in the main asteroid belt.

Acknowledgments

Various portions of this work were supported by NASA Planetary Geology and Geophysics Program grants NAG5-10345 and NAG5-13792 [MJG], by NASA Exobiology Program NSCORT grant NAG5-7598 to the New York Center for Studies on the Origins of Life [MJG], and by NASA Graduate Student Researchers Program grant NGT5-50382 [PSH]. The authors thank Ed Cloutis and Jessica Sunshine for their helpful comments and suggestions while reviewing this paper.

References

Adams, J.B., 1974. Visible and near-infrared diffuse reflectance spectra of pyroxenes as applied to remote sensing of solid objects in the Solar System. J. Geophys. Res. 79, 4829–4836.

Barucci, M.A., Capria, M.T., Coradini, A., Fulchignoni, M., 1987. Classification of asteroids using G-mode analysis. Icarus 72, 304–324.

Bell, J.F., Owensby, P.D., Hawke, B.R., Gaffey, M.J., 1988. The 52-color asteroid survey: final results and interpretations. Lunar Planet. Sci. 19. Abstract 57.

Brearley, A.J., Jones, R.H., 1998. Chondritic meteorites. In: Papike, J.J. (Ed.), Planetary Materials. Mineralogical Society of America, Washington, DC, pp. 3-1–3-398.

Brett, R., Sato, M., 1984. Intrinsic oxygen fugacity measurements on seven chondrites, a pallasite, and a tektite and the redox state of meteorite parent bodies. Geochim. Cosmochim. Acta 48, 111–120.

Burbine Jr., T.H., 1991. Principal component analysis of asteroid and meteorite spectra from 0.3 to 2.5 μm. Master's thesis. University of Pittsburgh, Pittsburgh.

Burns, R.G., 1993. Mineralogical Applications of Crystal Field Theory. Cambridge Univ. Press, Cambridge, UK.

Bus, S.J., 1999. Compositional structure in the asteroid belt: results of a spectroscopic survey. Doctoral thesis. Massachusetts Institute of Technology, Cambridge.

Bus, S.J., Binzel, R.P., 2002. Phase II of the small main-belt asteroid spectroscopic survey: the observations. Icarus 158, 106–145.

Campbell, A.J., Humayun, M., Weisberg, M.K., 2002. Siderophile element constraints on the formation of metal in the metal-rich chondrites Bencubbin, Weatherford, and Gujba. Geochim. Cosmochim. Acta 66, 647–660.

Chapman, C.R., Gaffey, M.J., 1979. Reflectance spectra for 277 asteroids. In: Gehrels, T. (Ed.), Asteroids. Univ. of Arizona Press, Tucson, pp. 655–687.

Chapman, C.R., Salisbury, J.W., 1973. Comparisons of meteorite and asteroid spectral reflectivities. Icarus 19, 507–522.

Clark, R.N., 1980. A large-scale interactive one-dimensional array processing system. Publ. Astron. Soc. Pacific 92, 221–224.

Clark, B.E., Bell, J.F., Fanale, F.P., 1995. Results of the seven-color asteroid survey: infrared spectral observations of $\sim$ 50-km size S-, K-, and M-type asteroids. Icarus 113, 387–402.

Clark, B.E., Hapke, B., Pieters, C., Britt, D., 2002. Asteroid space weathering and regolith evolution. In: Bottke Jr., W.F., Cellino, A., Paolicchi, P., Binzel, R.P. (Eds.), Asteroids III. Univ. of Arizona Press, Tucson, pp. 585–599.

Cloutis, E.A., Gaffey, M.J., 1991. Pyroxene spectroscopy revisited: spectral-compositional correlations and relationship to geothermometry. J. Geophys. Res. 96, 22809–22826.

Cloutis, E.A., Gaffey, M.J., Jackowski, T.L., Reed, K.L., 1986. Calibrations of phase abundance, composition, and particle size distribution for olivine–orthopyroxene mixtures from reflectance spectra. J. Geophys. Res. 91, 11641–11653.

Eaton, N., Green, S.F., McCheyne, R.S., Meadows, A.J., Veeder, G.J., 1983. Observations of asteroids in the 3- to 4-μm region. Icarus 55, 245–249.

Feierberg, M.A., Lebofsky, L.A., Larson, H.P., 1981. Spectroscopic evidence for aqueous alteration products on the surfaces of low-albedo asteroids. Geochim. Cosmochim. Acta 45, 971–981.

Gaffey, M.J., 1976. Spectral reflectance characteristics of the meteorite classes. J. Geophys. Res. 81, 905–920.

Gaffey, M.J., 2001. Asteroids: does space weathering matter? Lunar Planet. Sci. XXXII. Abstract 1587.

Gaffey, M.J., 2003. Observational and data reduction techniques to optimize mineralogical characterizations of asteroid surface materials. Lunar Planet. Sci. XXXIV. Abstract 1602.

Gaffey, M.J., McCord, T.B., 1979. Mineralogical and petrological characterizations of asteroid surface materials. In: Gehrels, T. (Ed.), Asteroids. Univ. of Arizona Press, Tucson, pp. 688–723.

Gaffey, M.J., Burbine, T.H., Binzel, R.P., 1993. Asteroid spectroscopy: progress and perspectives. Meteoritics 28, 161–187.

Gaffey, M.J., Cloutis, E.A., Kelley, M.S., Reed, K.L., 2002. Mineralogy of asteroids. In: Bottke Jr., W.F., Cellino, A., Paolicchi, P., Binzel, R.P. (Eds.), Asteroids III. Univ. of Arizona Press, Tucson, pp. 183–234.

Grimm, R.E., McSween Jr., H.Y., 1993. Heliocentric zoning of the asteroid belt by aluminum-26 heating. Science 259, 653–655.

Hardorp, J., 1978. The Sun among the stars. Astron. Astrophys. 63, 383–390.

Harris, A.W., Young, J.W., Dockweiler, T., Gibson, J., Poutanen, M., Bowell, E., 1992. Asteroid lightcurve observations from 1981. Icarus 95, 115–147.

Herbert, F., 1989. Primordial electrical induction heating of asteroids. Icarus 78, 402–410.

Herbert, F., Sonett, C.P., Gaffey, M.J., 1991. Protoplanetary thermal metamorphism: the hypothesis of electromagnetic induction in the protosolar wind. In: Sonett, C.P., Giampapa, M.S., Matthews, M.S. (Eds.), The Sun in Time. Univ. of Arizona Press, Tucson, pp. 710–739.

Hiroi, T., Sasaki, S., 2001. Importance of space weathering simulation products in compositional modeling of asteroids: 349 Dembowska and 446 Aeternitas as examples. Meteorit. Planet. Sci. 36, 1587–1596.

Howell, E.S., Merenyi, E., Lebofsky, L.A., 1994. Classification of asteroid spectra using a neural network. J. Geophys. Res. 99, 10847–10865.

Jones, T.D., Lebofsky, L.A., Lewis, J.S., Marley, M.S., 1990. The composition and origin of the C, P, and D asteroids: water as a tracer of thermal evolution in the outer belt. Icarus 88, 172–192.

Keil, K., 1989. Enstatite meteorites and their parent bodies. Meteoritics 24, 195–208.

Keil, K., 2000. Thermal alteration of asteroids: evidence from meteorites. Planet. Space Sci. 48, 887–903.

Lagerkvist, C.-I., Harris, A.W., Zappala, V., 1989. Asteroid lightcurve parameters. In: Binzel, R.P., Gehrels, T., Matthews, M.S. (Eds.), Asteroids II. Univ. of Arizona Press, Tucson, pp. 1162–1179.

Larson, H.P., Feierberg, M.A., Lebofsky, L.A., 1983. The composition of Asteroid 2 Pallas and its relation to primitive meteorites. Icarus 56, 398–408.

Lebofsky, L.A., Feierberg, M.A., Tokunaga, A.T., Larson, H.P., Johnson, J.R., 1981. The 1.7- to 4.2-μm spectrum of Asteroid 1 Ceres: evidence for structural water in clay minerals. Icarus 48, 453–459.

Lupishko, D.F., Belskaya, I.N., 1989. On the surface composition of the M-type asteroids. Icarus 78, 395–401.

Magri, C., Ostro, S.J., Rosema, K.D., Thomas, M.L., Mitchell, D.L., Campbell, D.B., Chandler, J.F., Shapiro, I.I., Giorgini, J.D., Yeomans, D.K., 1999. Mainbelt asteroids: results of Arecibo and Goldstone radar observations of 37 objects during 1980–1995. Icarus 140, 379–407.

McSween, H.Y., Bennett III, M.E., Jarosewich, E., 1991. The mineralogy of ordinary chondrites and implications for asteroid spectrophotometry 1991. Icarus 90, 107–116.

Mitchell, D.L., Ostro, S.J., Rosema, K.D., Hudson, R.S., Campbell, D.B., Chandler, J.F., Shapiro, I.I., 1995. Radar observations of Asteroids 7 Iris, 9 Metis, 12 Victoria, 216 Kleopatra, and 654 Zelinda. Icarus 118, 105–131.

Mittlefehldt, D.W., McCoy, T.J., Goodrich, C.A., Kracher, A., 1998. Nonchondritic meteorites from asteroidal bodies. In: Papike, J.J. (Ed.), Planetary Materials. Mineralogical Society of America, Washington DC, pp. 4-1–4-195.

Moroz, L.V., Fisenko, A.V., Semjonova, L.F., Pieters, C.M., Korotaeva, N.N., 1996. Optical effects of regolith processes on S-asteroids as simulated by laser shots on ordinary chondrite and other mafic materials. Icarus 122, 366–382.

Newson, H.E., Drake, M.J., 1979. The origin of metal clasts in the Bencubbin meteorite breccia. Geochim. Cosmochim. Acta 43, 689–707.

Noble, S.K., Pieters, C.M., Keller, L.P., 2004. Quantitative aspects of space weathering: implications for regolith breccia meteorites and asteroids. Lunar Planet. Sci. XXXV. Abstract 1301.

Ostro, S.J., Campbell, D.B., Shapiro, I.I., 1985. Mainbelt asteroids: dual-polarization radar observations. Science 229, 442–446.

Ostro, S.J., Hudson, R.S., Nolan, M.C., Margot, J.-L., Scheeres, D.J., Campbell, D.B., Magri, C., Giorgini, J.D., Yeomans, D.K., 2000. Radar observations of Asteroid 216 Kleopatra. Science 288, 836–839.

Petaev, M.I., Meibom, A., Krot, A.N., Wood, J.A., Keil, K., 2001. The condensation origin of zoned metal grains in Queen Alexandra Range 94411: implications for the formation of the Bencubbin-like chondrites. Meteorit. Planet. Sci. 39, 93–106.

Rayner, J.T., Toomey, D.W., Onaka, P.M., Denault, A.J., Strahlberger, W.E., Vacca, W.D., Cushing, M.C., Wang, S., 2003. SpeX: a medium resolution 0.8–5.5 micron spectrograph and imager for the NASA Infrared Telescope Facility. Publ. Astron. Soc. Pacific 155, 362–382.

Rivkin, A.S., Howell, E.S., Britt, D.T., Lebofsky, L.A., Nolan, M.C., Branston, D.D., 1995. Three-micron spectroscopic survey of M- and E-class asteroids. Icarus 117, 90–100.

Rivkin, A.S., Howell, E.S., Lebofsky, L.A., Clark, B.E., Britt, D.T., 2000. The nature of M-class asteroids from 3-micron observations. Icarus 145, 351–368.

Rivkin, A.S., Howell, E.S., Vilas, F., Lebofsky, L.A., 2002. Hydrated minerals on asteroids: the astronomical record. In: Bottke Jr., W.F., Cellino, A., Paolicchi, P., Binzel, R.P. (Eds.), Asteroids III. Univ. of Arizona Press, Tucson, pp. 235–253.

Rubin, A.E., Kallemyn, G.W., Wasson, J.T., Clayton, R.N., Mayeda, T.K., Grady, M., Verchovsky, A.B., Eugster, O., Lorenzetti, S., 2003. Formation of metal and silicate globules in Gujba: a new Bencubbin-like meteorite fall. Geochim. Cosmochim. Acta 67, 3283–3298.

Tedesco, E.F., Veeder, G.J., 1992. IMPS albedos and diameters catalog (FP 102). In: Tedesco, E.F., Veeder, G.J., Fowler, J.W., Chillemi, J.R. (Eds.), The IRAS Minor Planet Survey. Phillips Laboratory, Air Force Materiel Command, Hanscom Air Force Base, MA, pp. 243–285.

Tedesco, E.F., Williams, J.G., Matson, D.L., Veeder, G.J., 1989. A three-parameter asteroid taxonomy. Astron. J. 97, 580–606.

Tholen, D.J., 1984. Asteroid taxonomy from cluster analysis of photometry. Doctoral thesis. University of Arizona, Tucson.

Tholen, D.J., 1989. Asteroid taxonomic classifications. In: Binzel, R.P., Gehrels, T., Matthews, M.S. (Eds.), Asteroids II. Univ. of Arizona Press, Tucson, pp. 1139–1150.

Walker, D., Grove, T., 1993. Ureilite smelting. Meteoritics 28, 629–636.

Wasson, J.T., 1990. Ungrouped iron meteorites in Antarctica: origin of anomalously high abundance. Science 249, 900–902.

Weisberg, M.K., Prinz, M., Nehru, C.E., 1990. The Bencubbin chondrite breccia and its relationship to CR chondrites and the ALH85085 chondrite. Meteoritics 25, 269–279.

Weisberg, M.K., Prinz, M., Clayton, R.N., Mayeda, T.K., Sugiura, N., Zashu, S., Ebihara, M., 2001. A new metal-rich chondrite grouplet. Meteorit. Planet. Sci. 36, 401–418.

Williams, J.G., 1989. Asteroid family identifications and proper elements. In: Binzel, R.P., Gehrels, T., Matthews, M.S. (Eds.), Asteroids II. Univ. of Arizona Press, Tucson, pp. 1034–1072.

Xu, S., Binzel, R.P., Burbine, T.H., Bus, S.J., 1995. Small main-belt asteroid spectroscopic survey: initial results. Icarus 115, 1–35.

Zellner, B., Tedesco, E., Tholen, D.J., 1985. The eight-color asteroid survey: results for 589 minor planets. Icarus 61, 355–416.